Characteristics of compressive stress around dowel joint in concrete pavement system

Jiachen GUO[a] and Tak-Ming CHAN[a*]

Department of Civil and Environmental Engineering, The Hong Kong Polytechnic University, Hong Kong, China

* Corresponding author: tak-ming.chan@polyu.edu.hk

Abstract

Although Friberg's theoretical analysis is frequently used to analyse the dowel bar-concrete interaction in jointed plain concrete pavement (JPCP) system, the compressive stress concentration at top and bottom of the dowel slot cannot be explained with this theory. In this paper, two modifications including the elastic deformation of concrete support and the stress distribution factor considering the sinusoidal contact stress distribution are proposed to improve the Friberg's theoretical analysis. Modifications are then validated against elastic finite element analysis (FEA) results in terms of the contact stress distribution, the maximum compressive stress as well as the range of compression zone. To further investigate the maximum compressive stress at the joint surface, relevant parameters including the dowel bar diameter, the modulus of elasticity of concrete as well as the joint width are studied through elastic finite element analysis (FEA). Apart from proposing referenced moduli of dowel support, a close relationship between the modified modulus of dowel support and dowel bar diameter is also found and verified. Finally, differences between the Friberg's theoretical analysis and the modified method are summarised in a flow chart at the end of the paper.

Keywords

Modified modulus of dowel support, elastic deformation of concrete support, compressive stress concentration, sinusoidal contact stress distribution, stress distribution factor.

1. Introduction

Jointed plain concrete pavement (JPCP) systems are normally designed with contraction joints with a certain interval to control cracks induced by concrete shrinkage (Ioannides 2005, Tayabji et al. 2013a, Tayabji et al. 2013b, Sii *et al.* 2014, Novak *et al.* 2017, Vaitkus *et al.* 2019). Among these joints, epoxy-coated dowel bars are normally installed and regarded as effective loading transfer devices to transfer load between pavement slabs (Tayabji *et al.* 2012, Tayabji *et al.* 2013a, Tayabji *et al.* 2013b, Al-Humeidawi and Mandal 2014a, Al-Humeidawi and Mandal 2018, Yin *et al.* 2020, Zuzulova *et al.* 2020). In JPCP systems, an effective loading transfer is achieved through the bearing stress provided by stiff concrete support. But a higher bearing stress will be induced in concrete dowel slot and cause stress concentration related failure such as concrete crushing. Consequently, the effectiveness of loading transfer is impaired and the service life of the whole pavement system is shortened (Heinrichs *et al.* 1989, Channakeshava *et al.* 1993, Guo *et al.* 1995, Riad 2001, Zhou 2011, Mackiewicz 2015a). Therefore, to avoid premature failure caused by the concentrated bearing stress in concrete around the dowel bar, it is necessary to conduct comprehensive analysis of dowel-concrete interaction.

In addition to experimental tests, finite element analysis (FEA) is an effective tool to evaluate the structural performance of concrete pavement systems (Tabatabaie and Barenberg 1978, Tabatabaie and Barenberg 1980, Tayabji and Colley 1986, Channakeshava *et al.* 1993, Guo *et al.* 1995, Kuo *et al.* 1995, Davids 2001, Riad 2001, Maitra *et al.* 2009, Zhou 2011, Li *et al.* 2012, Mackiewicz 2015a, Mackiewicz 2015b, Sadeghi and Hesami 2018a, Hernández López *et al.* 2020, Mackiewicz and Szydło 2020). Several decades ago, due to less developed

computational systems, two-dimensional finite element models were preferred to assess the loading transfer of JPCP systems and common modelling techniques are introduced as follows

- Dowel bars were modelled by bending beam elements and interaction between dowel bar and concrete was simulated by incorporating contact elements (Guo *et al.* 1993, Zaman and Alvappillai 1995).
- Define a certain loading transfer efficiency in the finite element analysis (Huang and Wang 1973, Huang 1985, Mahboub *et al.* 2004).
- Adopt two-dimensional plate elements to model the concrete slab and beam elements to model the dowel bar; the interaction between dowel bar and concrete was modelled by using separated vertical springs (Tabatabaie and Barenberg 1978, Tayabji and Colley 1986, Tia *et al.* 1987, Nishizawa *et al.* 1989, Guo *et al.* 1995, Zaman and Alvappillai 1995).

With the development of high-speed computers, three-dimensional finite element analysis (FEA) methods were then used.

- Concrete pavement slabs were modelled by three-dimensional solid elements and dowel bars were modelled by beam elements. The dowel-concrete interaction was simulated by discrete vertical springs (Channakeshava *et al.* 1993, Kuo *et al.* 1995, Bhattacharya 2000, Davids 2001, Nishizawa et al. 2001, Davids *et al.* 2003, Kim and Hjelmstad 2003, Maitra *et al.* 2009).
- Concrete pavements and dowel bars were modelled by three-dimensional solid elements. Surface-to-surface contact was employed to model the dowel-concrete

interaction (Shoukry *et al.* 2002, Prabhu *et al.* 2007, Prabhu *et al.* 2009, Saxena *et al.* 2009, Shoukry *et al.* 2011, Zhou 2011, Li *et al.* 2012, Al-Humeidawi and Mandal 2014b, Mackiewicz 2015a, Mackiewicz 2015b, Priddy *et al.* 2015, Kim *et al.* 2018, Sadeghi and Hesami 2018a, Sadeghi and Hesami 2018b, Mackiewicz and Szydło 2020).

Among these modelling techniques, three-dimensional finite element analysis with the surface-to-surface contact was verified to be applicable in analyzing concentrated bearing stress of concrete around dowel bar. (Shoukry *et al.* 2002, Shoukry *et al.* 2011, Li *et al.* 2012, Mackiewicz 2015a, Priddy *et al.* 2015, Mackiewicz and Szydło 2020).

For the theoretical analysis of dowel-concrete interaction, it was firstly proposed by Friberg *et al.* (1939) with the application of the Timoshenko's infinite beam on Winkler foundation model (Timoshenko and Lessells 1925). However, in spite of wide applications, there are two main drawbacks need to be concerned and improved. The first issue is stress distribution in concrete dowel slot. The uniformly distributed supporting stress cannot support the fact that concrete crushing initiates at top and bottom of dowel slot. Then the second issue is the overestimation of vertical deformation at joint surface, which will then lead to unreliable predictions of the modulus of dowel support and the maximum compressive stress at joint surface. The modulus of dowel support proposed by Yoder and Witczak (1991) ranged from 8×10^{10} to 8×10^{11} N/m^3 and 4×10^{11} N/m^3 was usually adopted in the design. However, with different types of concrete and dowel bars, using the uniform value may lead to an inaccurate prediction.

The objective of this paper is to modify the Friberg's theoretical analysis in terms of two issues

mentioned above. The validity of modifications is assessed by comparing theoretical analysis results with data obtained from FEA. Then a detailed parametric analysis is also implemented with the modified Friberg's theoretical analysis and FEA in terms of the dowel bar diameter, the modulus of elasticity of concrete and the pavement joint width.

2. The Friberg's theoretical analysis

As stated in the introduction section, based on the Timoshenko's infinite beam on Winkler foundation model, Friberg *et al.* (1939) derived the relationship between the maximum vertical deformation at joint surface y_0 and the vertical load P_t as expressed in Equation (1) and (2):

$$y_0 = \frac{P_t}{4\beta^3 EI}(2 + \beta z) \tag{1}$$

$$\beta = \sqrt[4]{\frac{k_0 d}{4EI}} \tag{2}$$

where, z is the joint width between pavement slabs,is the transferred shear force, is the modulus of dowel support (N/mm^3), d is the dowel bar diameter,E is the modulus of elasticity of dowel bar,I is the moment of inertia of the dowel bar section.

In order to obtain k_0, in the Friberg's theoretical analysis, y_0 is firstly calculated by relative deflection between loaded and unloaded blocks. As shown in Figure 1, the relative deflection Δ_r consists of four components including the vertical deformation at joint surface y_0, the deformation due to the slope of the dowel bar zdy_0/dx, the flexural deformation $P_t z^3/12EI$ as well as the shear deflection δ.

[Figure 1 near here]To simplify the calculation, the flexural deformation and the deformation

due to the slope of dowel bar are always neglected (Friberg *et al.* 1939, Shoukry *et al.* 2002, Porter and Pierson 2007). Thus, Equation (3) is used to calculate y_0 and, after obtaining k_0 through Equations (1) and (2), the maximum concrete compressive stress σ_0 at joint surface is calculated by Equation (4).

$$y_0 = \frac{(\Delta_r - \delta)}{2} \tag{3}$$

$$\sigma_0 = k_0 y_0 \tag{4}$$

Where, $\delta = \lambda P_t z/AG$, A is the cross-section area of the dowel bar, λ is the circular dowel form factor equal to 10/9, G is the shear modulus.

3. The modified Friberg's theoretical analysis

As discussed in the introduction section, the discrepancy of the Friberg's theoretical analysis mainly comes from the inaccurate calculation of vertical deformation y_0 at joint surface and the unreliable stress distribution between dowel bar and concrete. Therefore, the Friberg's theoretical analysis will be improved from these two aspects.

3.1 *Elastic deformation of the concrete support*

In Friberg's theoretical analysis, the Winkler foundation modelled concrete support deforms uniformly under vertical loads as described in Figure 2. However, this uniform deformation cannot give the reasonable explanation for the severe compressive stress concentration at the top and bottom of dowel slot. Concentrated compressive stress is induced by an excessively localised deformation which is inconsistent with the uniform deformation of the Winkler

foundation model. As stressed in Figure 2(b), due to discontinuous deflections at points A and B, the deformation of the Winkler foundation contradicts the continuity assumption of deformable medium proposed in mechanics of elasticity (Boresi *et al.* 2010). Therefore, Figure 3(a) shows the overall deformation of the lower part of the elastic concrete support. The maximum vertical deformation y_0 at the centre of dowel slot will cause concentrated compressive stress. Following the deformation continuity, apart from deformation within dowel slot, surrounding concrete also deforms slightly under vertical loads.

[Figures 2, 3 near here]As the flexural deformation $P_t z^3/12EI$ and deformation due to the slope of dowel bar zdy_0/dx are not considered in the Friberg's theoretical analysis, according to Equation (3), the vertical deformation at joint surface is overestimated, which then leads to the underestimation of the modulus dowel support. Therefore, considering the deformation of the elastic concrete support, the vertical deformation at joint surface y_0 is determined by Equation (5) as can be seen in Figure 3(b). Where y_c and y_s are vertical deflections at centre and side of dowel slot, respectively.

$$y_0 = y_c - y_s \tag{5}$$

3.2 Stress distribution factor

Contact stress between the dowel bar and concrete is closely related to the deformation of the dowel slot. Under vertical load, the deflection of dowel bar relative to the side of dowel slot is equal to y_0. Figure 4 shows the deflection decomposition and θ is the angle between the horizontal line and the line from centroid of dowel bar to the contact point. Assuming no penetration between the dowel bar and concrete, the deformation of the dowel slot normal to

the contact surface is equal to $y_0 sin\theta$. Then the induced contact stress can be obtained by Equation (6) with the modified modulus of dowel support k_M. As shown in Figure 5, the vertical component of contact stress is determined by stress decomposition following Equation (7). And the total vertical force F_v offered by concrete is calculated through numerical integration as expressed in Equations (8) to (10), where r is the radius of dowel bar.

$$\sigma_p = k_M \cdot y_0 sin\theta \tag{6}$$

$$\sigma_v = \sigma_p sin\theta \tag{7}$$

$$F_v = \int_0^l \sigma_v \, dl \tag{8}$$

$$= \int_0^\pi k_M \cdot y_0 sin^2\theta \, r d\theta \tag{9}$$

$$= \frac{1}{2}\pi r \cdot k_M y_0 \tag{10}$$

With the same y_0 and F_v, the equivalent modulus of dowel support k_e of dowel bar supported by the Winkler foundation is determined through Equations (11) and (12). $4/\pi$ can be regarded as a stress distribution factor considering the sinusoidal contact stress distribution. Therefore, to determine k_M, the maximum joint deformation y_0 is firstly determined by Equation (5). Similar to the Friberg's theoretical analysis, Equations (1) and (2) are used to calculate k_e. Then the stress distribution factor $4/\pi$ is incorporated to obtain k_M. Finally, the maximum compressive stress at joint surface is determined by Equation (4) with k_0 replaced by k_M.

$$F_v = \frac{1}{2}\pi r \cdot k_M y_0 = 2r \cdot k_e y_0 \tag{11}$$

$$k_M = \frac{4}{\pi} k_e \tag{12}$$

[Figures 4, 5 near here] **Finite element analysis**

As the bearing stress is concentrated at a relatively small area on the top and bottom of dowel slot, it is difficult to determine the magnitude of the compressive stress at joint surface through experimental tests (Al-Humeidawi and Mandal 2014b). Therefore, FEA is adopted to study the compressive stress concentration in dowel slot by using commercially available software ABAQUS (2014). Available numerical data are then used to verify the modifications of Friberg's theoretical analysis. Since both Friberg's theoretical analysis and the modified method investigate the dowel-concrete interaction by elastic analysis, all components in FEA are modelled with linear-elastic materials.

4.1 Model configuration

The configuration of the finite element model complies with the modified AASHTO T253 method as shown in Figure 6 (Porter et al. 2001, 2006, Porter and Pierson 2007). Following the common concrete pavement thickness and dowel bar spacing (AASHTO 1993, Tayabji *et al.* 2013a, Smith and Snyder 2019), the width and thickness of concrete blocks were 300 mm and 250 mm, respectively. The length of the unloaded block was 300 mm while that of loaded block was 600 mm. Dowel bars with 460 mm length was adopted in FEA while the dowel bar diameter was a considered parameter ranging from 24 mm to 38 mm. Joint width from 3.2 mm (1/4 in) to 12.7 mm (1/2 in) were investigated to meet the requirement of pavement design codes (AASHTO 1993, Tayabji *et al.* 2013, ACI Committee 325 2002).

[Figure 6 near here]

Both concrete blocks and steel dowel bar are modelled by three-dimensional eight-node solid elements with reduced integration (C3D8R). To reduce the computational efforts, symmetric constraints were adopted along both X and Z direction. Figure 7 presents the symmetric constraints as well as boundary conditions of unloaded blocks. U1, UR1, U2, UR2, U3 as well as UR3 are displacement and rotation along X, Y and Z axes, respectively. Then for the loading arrangement, as shown in Figure 7(d), a uniformly distributed load was applied at joint surface with 50 mm width.

[Figure 7 near here]***Materials***

To show the consistency with the Friberg's theoretical analysis and the modified method, linear-elastic material properties are used to model both the steel dowel bar and concrete blocks. Table 1 lists elastic material properties of concrete and steel. A total three types of normal strength concrete (NSC) C-I, C-II and C-III with the modulus of elasticity 29.7, 33.0 as well as 36.0 GPa are included following the FIB Model Code for Concrete Structures 2010 (Taerwe and Matthys 2013). The modulus of elasticity of the steel dowel bar adopted in the FEA is 210.0 GPa (Riad 2001, Shoukry *et al.* 2002, Zhou 2011, Al-Humeidawi and Mandal 2014b, Priddy *et al.* 2015).

[Table 1 near here]

4.3 Model validation

The finite sliding, surface-to-surface contact formulation technique was used to establish interaction between the dowel bar and concrete (Riad 2001, Shoukry *et al.* 2002, Prabhu et al. 2009, Zhou 2011, Li *et al.* 2012, Sii et al. 2014, Al-Humeidawi and Mandal 2014b, Al-

Humeidawi and Mandal 2022). Compared with the concrete block and dowel bar modelled by linear elastic materials, the accuracy of models depended more on the contact simulation between these two components.

Therefore, the effectiveness of the surface-to-surface contact modelling technique was validated against test results of the stainless steel ring strengthened removable dowel bar connection system (Guo and Chan 2022). To simulate the localised concrete crushing failure, concrete damaged plasticity (CDP) model in ABAQUS was adopted to simulate complex plastic deformations of concrete. Relevant parameters including dilation angle ψ, equibiaxial compressive stress to uniaxial compressive stress σ_{b0}/f_{c0}, tensile meridian to compressive meridian K, eccentricity ϵ and viscosity parameter were defined from the ABAQUS user manual (2014) and equal to 38°, 1.16, 0.667, 0.1 as well as zero, respectively. Other details of CDP model can be found in the FEA conducted by Guo and Chan (2022). As presented in Figure 8(a), the localised concrete crushing failure was well simulated with concrete compressive damage variables d_c in model 32D, 32D4T as well as 32D4T10R100L. Besides, load-deflection relationships from FEA also matched those from experimental tests as plotted in Figure 8(b). For specimens 32D4T and 32D4T10R100L, slight differences of initial stiffnesses between experimental tests and FEA were due to gaps between different components. However, predicted ultimate loads by FEA were almost the same as those obtained in the experimental test.

The validity of elastic models can also be verified with field test data collected by the falling weight deflectometer (FWD) along the middle line of the concrete pavement (Mackiewicz,

2015(b)). The corresponding jointed concrete pavement model is shown in Figure 9(a). All components were modelled with linear elastic materials with moduli of elasticity as well as Poisson's ratios summarised in Table 2. The dowel-concrete interaction as well as the contact between concrete slab and subbase layer were modelled by surface-to-surface contact with finite sliding. While the subbase, the protection layer as well as the subgrade were tied together. Apart from the fixed constraint at the bottom surface of the subgrade layer, a symmetric constraint was set along X direction. The vertical load was exerted by a circular steel plate with uniform pressure equal to 0.7 MPa.

Deflection responses of pavement slabs and load-deflection curves obtained from FWD test as well as FEA are plotted in Figure 9(b, c). It could be found that deflections of loaded as well as unloaded pavements predicted by FEA show close matches to those obtained from FWD field test and FEA conducted by Mackiewicz (2015b).

[Figure 8, 9 near here]

[Table 2 near here]***Mesh convergence analysis***

Although the displacement-based mesh convergence analysis was frequently adopted in previous research (Al-Humeidawi and Mandal 2014b, Mackiewicz 2015b, Mackiewicz and Szydło 2020), a convergent vertical displacement did not mean the convergency of stress. As the main objective of this study was to evaluate the maximum compressive stress at joint surface, the stress-based mesh convergence analysis should also be conducted. In Figure 10, it could be found that the maximum vertical deflection of dowel slot in the unloaded concrete block showed convergency when mesh size is smaller than 5 mm. While the maximum contact

stress only presented a convergent trend when mesh size was smaller than 1 mm. As can be seen from Figure 10 and Figure 11, vertical compressive stress (S22) was equal to the normal contact stress (CPRESS) when the mesh size was extremely small. Therefore, 0.5 mm was optioned as local mesh size with difference smaller than 5% between contact stress and vertical compressive stress.

[Figure 10 and 11 near here]***Validation of the modified Friberg's theoretical analysis***

The Friberg's theoretical analysis has been improved considering the elastic deformation of concrete support and stress distribution factor as discussed in sections 3.1 and 3.2. To validate these modifications, comparisons among the Friberg's theoretical analysis, the modified method as well as FEA results were conducted in terms of the contact stress distribution, the maximum compressive stress at joint surface as well as the range of compression zone.

5.1 Contact stress distribution

The distribution of contact stress in the dowel slot of the unloaded concrete block analysis can be plotted by setting a path in FEA. Figure 12(a) shows the created path along dowel slot in the unloaded block. Then for the contact distribution predicted by the Friberg's theoretical analysis and the modified method, relevant deflection data were firstly obtained from FEA as presented in Figures 12(b) and 12(c) including Δ_r, y_c and y_s. Then with these deflection data, y_0 was calculated by Equations (3) and (5) for the Friberg's theoretical analysis and the modified method, respectively. After that, Equations (1) and (2) were used to determine k_0 and k_e. Then k_M was obtained after considering the stress distribution factor as expressed in Equation (12). Finally, σ_0 was calculated by Equation (4) with k_0 and k_M in the Friberg's theoretical analysis

and the modified method, respectively. To avoid the peak stress exceeding the compressive strength of NSC, 5 kN was treated as a referenced load and the distribution of contact stress of models with 12.7 mm joint width and C-I concrete is plotted in Figure 13. Compared with the uniformly distributed contact stress according to the Friberg's theoretical analysis, the modified method provided more accurate predictions in terms of the contact stress distribution and the peak stress value.

[Figure 12 and 13 near here.]

5.2 Maximum compressive stress

Under 5 kN referenced load, the maximum compressive stress σ_0 in unloaded block predicted by the Friberg's theoretical analysis and the modified method were compared with that obtained from FEA as depicted in Figure 14. Choosing the standard 32 mm diameter dowel bar as an example, Table 3 summarises σ_0 of models with different joint widths and types of concrete. The stress ratio in the table means the predicted σ_0 over that obtained from FEA. It was found that maximum compressive stresses obtained from the Friberg's theoretical analysis were far from those from FEA with stress ratios ranging from 0.56 to 0.61. However, after improvements, the modified method can almost achieve 90 percent predictions as listed in the last column of Table 3. Besides, it was reasonable that the modulus of dowel support is an inherited parameter that independent of the joint width (Yin et al. 2020). This deduction can also be validated by k_M calculated by the modified method as presented in Table 3.

[Table 3 near here]

[Figure 14 near here]

5.3 Range of compression zone

In Friberg's theoretical analysis and the modified method, induced compressive stress was proportional to the vertical deformation as indicated in Equation (4). Based on Timoshenko's infinite beam on the Winkler foundation model, the vertical deformation of dowel slot *y* can be expressed as Equation (13), where *x* is the distance between joint surface and the contact point. The range of compression zone, namely the distance between joint surface and zero-compressive-stress point, was then determined by Equation (14). The longitudinal distribution of compressive stress along dowel slot in FEA can be plotted by creating a path along the center of dowel slot as shown in Figure 15. Therefore, to further validate the modifications of the Friberg's theoretical analysis, Figure 16 compares distributions of compressive stress predicted by the Friberg's theoretical analysis, the modified method and FEA. It could be seen that longitudinal distributions of compressive stress predicted by the Friberg's theory significantly deviate from those obtained from FEA. The underestimation of the maximum compressive stress σ_0 and the overestimation of the range of compression zone cannot give a clear insight into the compressive stress concentration within dowel slot. While the range of compression zone calculated by the modified method was more accurate. Differences were less than 4 percent for models with the standard 32 mm diameter dowel bar as indicated in Table 4.

$$y = \frac{e^{-\beta x}}{4\beta^3 EI}[2P_t cos\beta x + \beta P_t z(cos\beta x - sin\beta x)] \tag{13}$$

$$x = arctan\left(1 + \frac{2}{\beta z}\right)/\beta \tag{14}$$

[Figure 15 and 16 near here]

[Table 4 near here]**Parametric analysis**

From both FEA and theoretical analysis, apart from the modulus of elasticity of the dowel bar, the maximum compressive stress at the joint surface σ_0 is also influenced by several factors including the dowel bar diameter, joint width as well as the modulus of elasticity of concrete. The following parametric analysis is carried out to study σ_0 in terms of these affected parameters.

6.1 Dowel bar diameter

For models with C-I concrete and 6.4 mm joint width, Figure 17 plots the longitudinal compressive stress distribution along dowel slot with dowel bar diameters from 24 mm to 38 mm. Under 5 kN referenced load, the maximum vertical compressive stress in the model with a 24 mm diameter dowel bar and 6.4 mm joint width was -30.45 MPa. However, for models with a 32 mm and 38 mm dowel bar, maximum vertical compressive stresses at joint surface were only -16.42 MPa and -11.66 MPa, respectively. Then the range of compression zone of the model with a 24 mm diameter dowel bar is only 33 mm. While those with a 32 mm and 38 mm dowel bar were expanded to 44 mm and 53 mm, respectively. To clearly describe the range of compression zone and assess the compressive stress concentration within dowel slot, Figure 18 plots three-dimensional contact stress distribution regarding models with C-I concrete and 12.7 mm joint width. X coordinate is the hoop distance between dowel side and contact point; Y coordinate is the longitudinal distance from joint surface to contact point; And Z coordinate indicates the normal contact stress. It can be seen that the application of a large diameter dowel bar not only enlarges the contact area between dowel bar and concrete, but also expands the

compression zone. Therefore, under heavy wheel loads, large diameter dowel bars are suggested to relieve compressive stress concentration at joint surface.

[Figure 17, 18 near here]***Modulus of elasticity of concrete***

Modulus of elasticity of concrete is also an important parameter influencing the maximum compressive strength at joint surface. Maximum compressive stresses of models with different types of concrete and dowel bar diameters can be found in Table 5. From Figure 19, the maximum compressive stress at the joint surface σ_0 increased with the modulus of the elasticity of concrete. This was because the stiffness of the concrete support increases with the concrete modulus of elasticity and a smaller compression zone is then created according to Equations (2) and (14). As a result, compressive stress concentration became more severe with higher compressive stress created at joint surface.

[Figure 19 near here]

[Table 5 near here]***Joint width***

In parametric analysis, 3.2 mm, 6.4 mm as well as 12.7 mm were considered and studied. C-I type concrete was chosen as the reference to assess effects of joint widths. Figure 20 plots relationships between joint widths and vertical compressive stresses. Based on Equation (4), a large joint width led to an extra deformation at the joint surface and therefore induced a higher compressive stress. From Equations (1) and (2), the induced vertical deformation was inversely proportional to the diameter of the dowel bar. And the modulus of dowel support was reduced with the diameter as summarised in Table 6. As a result, for models with a large diameter dowel bar, lower deformations and compressive stress increments were caused compared with models

with a small diameter dowel bar. Table 7 shows maximum vertical stresses and stress increments with different joint widths. The stress increment for the model with a 24 mm diameter dowel bar was -5.72 MPa. In contrast, stress increments for models with 32 mm and 38 mm diameter dowel bars were only -2.56 MPa and -1.58 MPa, respectively. Narrow joints are preferred in the design of jointed concrete pavements once meeting the requirement of free sliding of pavement slabs.

[Figure 20 near here]

[Table 6, 7 near here]**Proposed moduli of dowel support**

The maximum compressive stress at joint surface is related to the modulus of dowel support. As discussed and proved in section 5.2, the modulus of dowel support was an inherited property which is independent from the joint width. Therefore, to accurately determine the maximum compressive stress, Table 8 summarises modified moduli of dowel support k_M calculated with deflection data obtained from FEA. In the Friberg's theoretical analysis, the reaction of dowel support k was replaced by $k_0 d$. If Timoshenko's infinite beam model is applicable to analyse the structural performance of the dowel bar, the product of the modulus of dowel support and dowel bar diameter should be the same as Equation (15) indicates. where,are moduli of dowel support corresponding to dowel bar diameters equal to d_1 and d_2, respectively.

$$k_1 d_1 = k_2 d_2 \tag{15}$$

Table 9 concludes the reaction of dowel support ($k_e d$) of each model. And relationships between dowel bar diameters and reactions of dowel support are displayed in Figure 21. It was noted that reactions of dowel support are almost independent of dowel bar diameters and only

influenced by moduli of elasticity of concrete.

[Figure 21 near here]

[Table 7, 8 near here]**Comparison between the Friberg's theoretical analysis and the modified method**

A simplified flow chart is drawn in Figure 22 to show two main differences between the Friberg's theoretical analysis and the modified method. The first difference was the determination of the vertical deformation y_0 at joint surface. In the Friberg's theoretical analysis, y_0 was calculated by Equation (3) which ignores the flexural deformation and deformation due to the dowel bar slope. Because of this, the calculated vertical deformation at joint surface was overestimated. While in the modified method, the elastic deformation of concrete support was considered and y_0 was determined by Equation (5). Then the second difference was the stress distribution factor which is proposed in the modified method to consider the sinusoidal contact stress distribution within dowel slot. After incorporating these two modifications, the prediction of the maximum compressive stress was enhanced from 55 percent to 90 percent. With the application of the modified method, a close relationship between the modulus of dowel support and dowel bar diameter was also found and verified as Equation (15) shows.

[Figure 22 near here]

9. Conclusions

This paper firstly modified the original Friberg's theoretical analysis from contact stress distribution and deformation of concrete support these two aspects. Modifications were then validated by comparing results from elastic FEA with those predicted by the Friberg's

theoretical analysis and the modified method. After comparisons, the modified Friberg's theoretical analysis was proved to be more accurate than the original method in the following aspects.

(1) The sinusoidal contact stress distribution derived in the modified Friberg's theoretical analysis showed close match to the contact stress distribution in FEA.

(2) The maximum compressive stress at joint surface calculated by the modified Friberg's theoretical analysis was closer to that obtained from FEA.

(3) The modified Friberg's theoretical analysis predicted a more precise range of compression zone.

(4) The modified modulus of dowel support was found to be independent of the joint width, which was consistent with the deduction proposed by other researchers.

Then through a comprehensive parametric analysis, it was found that the maximum compressive stress at joint surface increases with the modulus of elasticity of concrete as well as joint width but reduces with the dowel bar diameter. Then with deflection data generated from FEA, referenced moduli of dowel support were proposed and a close relationship was found with the dowel bar diameter.

Disclosure statement

No potential conflict of interest was reported by the author(s).

References

American Association of State Highway and Transportation Officials, 1993. Guide for design of pavement structure. Washington D.C: AASHTO.

ABAQUS, Dassault Systems, Waltham, MA, USA, 2014.

ABAQUS. 6.14, CAE User's Guide. Dassault Systems 2014.

ACI Committee 325, 2002. ACI 325.12R-02 Guide for design of jointed concrete pavements for streets and local roads. American Concrete Institute, Detroit, MI.

Al-Humeidawi, B. H. and Mandal, P., 2014a. Evaluation of performance and design of GFRP dowels in jointed plain concrete pavement–part 1: experimental investigation. *International Journal of Pavement Engineering,* 15(5), 449-459.

Al-Humeidawi, B. H. and Mandal, P., 2014b. Evaluation of performance and design of GFRP dowels in jointed plain concrete pavement–part 2: numerical simulation and design considerations. *International Journal of Pavement Engineering,* 15(8), 752-765.

Al-Humeidawi, B. H. and Mandal, P., 2018. Experimental investigation on the combined effect of dowel misalignment and cyclic wheel loading on dowel bar performance in JPCP. *Engineering Structures,* 174, 256-266.

Al-Humeidawi, B. H. and Mandal, P. 2022. Numerical evaluation of the combined effect of dowel misalignment and wheel load on dowel bars performance in JPCP. *Engineering Structures*, 252, 113655.

Bhattacharya, K., 2000. Nonlinear response of transverse joints of airfield pavements. *Journal of Transportation Engineering,* 126(2), 168-177.

Boresi, A P., Chong, K, Lee, J. D., 2010. Elasticity in engineering mechanics. New Jersey: John Wiley & Sons.

Channakeshava, C., Barzegar, F. and Voyiadjis, G. Z., 1993. Nonlinear FE analysis of plain concrete pavements with doweled joints. *Journal of Transportation Engineering,* 119(5), 763-781.

Davids, W. G., 2001. 3D finite element study on load transfer at doweled joints in flat and curled rigid pavements. *International Journal of Geomechanics,* 1(3), 309-323.

Davids, W. G.*, et al.*, 2003. Three-dimensional finite element analysis of jointed plain concrete pavement with EverFE2. 2. *Transportation Research Record,* 1853(1), 92-99.

Friberg, B., Richart, F. and Bradbury, R., 1939. Load and deflection characteristics of dowels in transverse joints of concrete pavements. *Highway Research Board Proceedings*.

Guo, H., Larson, R. and Snyder, M., 1993. A nonlinear mechanistic model for dowel looseness in PCC pavements. *Fifth International Conference on Concrete Pavement Design and Rehabilitation*. Purdue University, School of Civil Engineering.

Guo, H., Sherwood, J. A. and Snyder, M. B., 1995. Component dowel-bar model for load-transfer systems in PCC pavements. *Journal of Transportation Engineering,* 121(3), 289-298.

Guo, J. C., Chan, T-M., 2022. Experimental and numerical study on the structural performance of the stainless steel ring strengthened removable dowel bar connection system. *International Journal of Pavement Engineering.*(Uunder Review)

Heinrichs, K. W.*, et al.*, 1989. *Rigid pavement analysis and design.* United States. Federal

Highway Administration.

Hernández López, F. M., *et al.*, 2020. 3D-FE of jointed plain concrete pavement over continuum elastic foundation to obtain the edge stress. 19(1), 5-18.

Huang, Y., and Wang, S, 1973. Finite-element analysis of concrete slabsand its implications for rigid pavement design. Highway Research Record, 466, 55–69.

Huang, Y. H., 1985. A computer package for structural analysis of concrete pavements. *Third International Conference on Concrete Pavement Design and Rehabilitation. Purdue University, School of Civil Engineering; Federal Highway Administration; Portland Cement Association; Transportation Research Board; Federal Aviation Administration; and Indiana Department of Highways*.

Ioannides, A. M., 2005. Stress prediction for cracking of jointed plain concrete pavements, 1925–2000: an overview. *Transportation Research Record,* 1919(1), 47-53.

Kim, J. and Hjelmstad, K. D., 2003. Three-dimensional finite element analysis of doweled joints for airport pavements. *Transportation Research Record,* 1853(1), 100-109.

Kim, K., *et al.*, 2018. Effect of dowel bar arrangements on performance of jointed plain concrete pavement (JPCP). *International Journal of Concrete Structures,* 12(1), 1-11.

Kuo, C-M., Hall, K. T., and Darter, M. I, 1995.Three-dimensional finite element model for analysis of concrete pavement support.Transportation Research Record, 1505, 119–127.

Li LK, *et al.*, 2012. Characterization of Contact Stresses Between Dowels and Surrounding Concrete in Jointed Concrete Pavement.

Mackiewicz, P., 2015a. Analysis of stresses in concrete pavement under a dowel according to

its diameter and load transfer efficiency. *Canadian Journal of Civil Engineering,* 42(11), 845-853.

Mackiewicz, P., 2015b. Finite-element analysis of stress concentration around dowel bars in jointed plain concrete pavement. *Journal of Transportation Engineering,* 141(6), 06015001.

Mackiewicz, P. and Szydło, A., 2020. The analysis of stress concentration around dowel bars in concrete pavement. *Magazine of Concrete Research,* 72(2), 97-107.

Mahboub, K. C., Liu, Y. and Allen, D. L., 2004. Evaluation of temperature responses in concrete pavement. *Journal of Transportation Engineering,* 130(3), 395-401.

Maitra, S. R., Reddy, K. and Ramachandra, L., 2009. Load transfer characteristics of dowel bar system in jointed concrete pavement. *International Journal of Fracture,* 135(11), 813-821.

Nishizawa, T., Fukuda, T. and Matsuno, S., 1989. A Refined Model of Doweled Joints for Concrete Pavement Using FEM Analysis. *Proceedings, 4th International Conference on Concrete Pavement Design and Rehabilitation, Purdue University.*

Nishizawa, T.*, et al.*, 2001. Study on mechanical behavior of dowel bar in transverse joint of concrete pavement. *Proceedings of the 7th International Conference on Concrete Pavements, Orlando*.

Novak, J.*, et al.*, 2017. Precast concrete pavement–systems and performance review. *IOP Conference Series: Materials Science and Engineering*, 012030.

Porter, M. and Pierson, N. 2007. Laboratory evaluation of alternative dowel bars for use in

Portland cement concrete pavement construction. *Transportation Research Record,* 2040(1), 80-87.

Porter, M. L.*, et al.*, 2006. *Laboratory study of structural behavior of alternative dowel bars.*

Porter, M. L., Guinn Jr, R. J. and Lundy, A. L., 2001. Dowel bar optimization: Phases I and II.

Prabhu, M., Varma, A. H. and Buch, N., 2007. Experimental and analytical investigations of mechanistic effects of dowel misalignment in jointed concrete pavements. *Transportation Research Record,* 2037(1), 12-29.

Prabhu, M., Varma, A., and Buch, N, 2009. Analytical investigation of the effects of dowel misalignment on concrete pavement joint opening behaviour. International Journal of Pavement Engineering, 10 (1), 49–62.

Priddy, L. P.*, et al.*, 2015. Three-dimensional modelling of precast concrete pavement repair joints. *Magazine of Concrete Research,* 67(10), 513-522.

Riad, M. Y., 2001. Stress concentration around dowel bars in jointed rigid concrete pavements.

Sadeghi, V. and Hesami, S., 2018a. Finite element investigation of the joints in precast concrete pavement. *Computers Concrete,* 21(5), 547-557.

Sadeghi, V. and Hesami, S., 2018b. Investigation of load transfer efficiency in jointed plain concrete pavements (JPCP) using FEM. *International Journal of Pavement Research Technology,* 11(3), 245-252.

Saxena, P.*, et al.*, 2009. Laboratory and finite element evaluation of joint lockup. *Transportation Research Record,* 2095(1), 34-42.

Shoukry, S. N., William, G. and Riad, M., 2002. Characteristics of concrete contact stresses in

doweled transverse joints. *International Journal of Pavement Engineering,* 3(2), 117-129.

Shoukry, S. N., William, G. W. and Riad, M., 2011. Application of LS-DYNA in Identifying Critical Stresses Around Dowel Bars. *8th Int. LS-DYNA Users Conference*.

Sii, H. B., et al., 2014. Development of prediction model for doweled joint concrete pavement using three-dimensional finite element analysis. Applied Mechanics and Materials, 587, 1047–1057.

Smith, P., and Snyder, M. B, 2019. Manual for jointed precast concrete pavement. Carmel, IN: National Precast Concrete Association.

Tabatabaie, A. M., and Barenberg,E, 1978. Finite-element analysis of jointed or cracked concrete pavements.Transportation Research Record, 671, 11–19.

Tabatabaie, A. M. and Barenberg, E. J., 1980. Structural analysis of concrete pavement systems. *Transportation Engineering Journal of Asce,* 106(5), 493-506.

Taerwe, L., and Matthys, S, 2013. Fib model code for concrete structures 2010. Berlin, Germany:Ernst & Sohn, Wiley.

Tayabji, S. D. and Colley, B. E., 1986. Analysis of jointed concrete pavements.

Tayabji, S., Ye, D. and Buch, N. 2012. Joint load transfer and support considerations for jointed precast concrete pavements. Transportation Research Record, 2305(1), 74-80.

Tayabji, S., Ye, D., and Buch, N, 2013a. Precast concrete pavement technology. Washington:Transportation Research Board.

Tayabji, S., Ye, D., and Buch, N, 2013b. Precast concrete pavements: technology overview and

technical considerations. Pci Journal, 58 (1), 112–128.

Tia, M., et al., 1987. FEACONS III computer program for analysis of jointed concrete pavements.Transportation Research Record, 1136 (1), 12–22.

Timoshenko, S., and Lessells, J. M., 1925. Applied elasticity.East Pittsburgh: Westinghouse technical night school press.

Vaitkus, A.*, et al.*, 2019. Concrete modular pavements–types, issues and challenges. *The Baltic Journal of Road Bridge Engineering,* 14(1), 80-103.

Yin, W., et al., 2020. Mechanical characteristics of dowel bar-concrete interaction: based on substructure experiment. International Journal of Pavement Engineering, 23 (7), 2392–2404.

Yoder,E. J., and Witczak, M. W, 1991. Principles of pavement design. New York: John Wiley.

Zaman, M. and Alvappillai, A., 1995. Contact-element model for dynamic analysis of jointed concrete pavements. *Journal of Transportation Engineering,* 121(5), 425-433.

Zhou, Z., 2011. Stress concentration analysis in concrete round dowels for airport jointed rigid pavement system. *ICTE 2011.* 1566-1571.

Zuzulova, A., Grosek, J. and Janku, M., 2020. Experimental laboratory testing on behavior of dowels in concrete pavements. *Materials,* 13(10), 2343.

Table 1 Material properties adopted in finite element analysis.

Material	Modulus of elasticity (GPa)	Poisson's ratio, ν
Steel	210.0	0.3
C-I	29.7	0.2
C-II	33.0	0.2
C-III	36.0	0.2

Table 2 Material parameters in the finite element analysis.

Component ID	Modulus of elasticity (MPa)	Poisson's ratio
Concrete slab	35,000	0.2
Dowel bar	210,000	0.3
Subbase	2900	0.3
Protection layer	193	0.35
Subgrade	143	0.35

Table 3 Maximum compressive stresses at joint surface (σ_0).

Joint width (mm)	E_c (GPa)	$\sigma_{0,FE}$ (MPa)	k_0 (N/mm^3)	$\sigma_{0,Friberg}$ (MPa)	Stress ratio	k_M (N/mm^3)	$\sigma_{0,Modified}$ (MPa)	Modified Stress ratio
3.2	29.7	15.55	981.77	9.51	0.61	2192.64	14.14	0.91
6.4	29.7	16.42	942.04	9.90	0.60	2192.64	14.82	0.90
12.7	29.7	18.11	830.06	10.26	0.57	2218.85	16.33	0.90
3.2	33.0	16.16	1093.87	9.81	0.61	2437.17	14.53	0.90
6.4	33.0	17.09	1036.68	10.09	0.59	2437.17	15.28	0.89
12.7	33.0	18.89	929.07	10.67	0.56	2437.17	16.70	0.88
3.2	36.0	16.69	1199.59	10.09	0.60	2641.07	14.81	0.89
6.4	36.0	17.67	1138.28	10.42	0.59	2641.07	15.58	0.88
12.7	36.0	19.57	1008.95	10.95	0.56	2671.21	17.26	0.88

Table 4 Ranges of compression zone.

Joint width (mm)	E_c (GPa)	The range of compression zone (FE) (mm)	The range of compression zone (Friberg) (mm)	Length ratio (Friberg)	The range of compression zone (Modified) (mm)	Length ratio (Modified)
3.2	29.7	47	52.27	1.11	45.23	0.96
6.4	29.7	44	51.43	1.17	43.87	1.00
12.7	29.7	41	50.75	1.24	41.43	1.01
3.2	33.0	44	50.83	1.13	44.02	0.98
6.4	33.0	42	50.15	1.17	42.66	0.99
12.7	33.0	40	49.22	1.20	40.38	0.98
3.2	36.0	43	49.64	1.13	43.11	0.98

6.4	36.0	41	48.93	1.17	41.76	0.99
12.7	36.0	39	48.12	1.23	39.37	1.01

Table 5 Maximum vertical compressive stresses with different types of concrete (12.7 mm joint width).

Dowel bar diameter (mm)	Concrete type	The maximum vertical compressive stress (MPa)
24	C-I	-33.01
24	C-II	-34.41
24	C-III	-35.65
32	C-I	-18.11
32	C-II	-18.89
32	C-III	-19.57
38	C-I	-12.7
38	C-II	-13.25
38	C-III	-13.72

Table 6 Moduli of dowel support with different dowel bar diameters.

Dowel diameter (mm)	Joint width (mm)	E_c (GPa)	k_0 (N/mm^3)	k_M (N/mm^3)
24	3.2	29.7	1251.72	2815.41
24	6.4	29.7	1166.83	2833.22
24	12.7	29.7	989.21	2853.67
32	3.2	29.7	981.77	2192.64
32	6.4	29.7	942.04	2192.64
32	12.7	29.7	830.06	2218.85
38	3.2	29.7	869.31	1900.59
38	6.4	29.7	828.17	1900.59
38	12.7	29.7	750.28	1900.59

Table 7 Maximum vertical compressive stresses with joint widths ($\sigma_{0,FE}$) (C-I concrete).

Dowel bar diameter (mm)	Joint width (mm)	$\sigma_{0,FE}$ (MPa)	Stress increment (MPa)
24	3.2	-27.29	
24	6.4	-29.24	-1.95
24	12.7	-33.01	-5.72
32	3.2	-15.55	
32	6.4	-16.42	-0.87
32	12.7	-18.11	-2.56
38	3.2	-11.12	
38	6.4	-11.66	-0.54
38	12.7	-12.70	-1.58

Table 8 Proposed moduli of dowel support.

Dowel bar diameter (mm)	Steel modulus of elasticity (GPa)	Concrete modulus of elasticity (GPa)	k_M (N/mm^3)
		29.7	2840
24	210.0	33.0	3140
		36.0	3430
		29.7	2640
26	210.0	33.0	2930
		36.0	3180
		29.7	2460
28	210.0	33.0	2720
		36.0	2980
		29.7	2290
30	210.0	33.0	2570
		36.0	2830
		29.7	2190
32	210.0	33.0	2430
		36.0	2650
		29.7	2100
34	210.0	33.0	2330
		36.0	2530
		29.7	1960
36	210.0	33.0	2180
		36.0	2410
		29.7	1900
38	210.0	33.0	2100
		36.0	2290

Table 9 Reactions of dowel support $k_e d$.

Dowel bar diameter (mm)	Concrete modulus of elasticity (GPa)	Equivalent modulus of dowel support k_e (N/mm^3)	Reaction of dowel support $k_e d$ (N/mm^2)
24	29.7	2230	53520
26	29.7	2070	53820
28	29.7	1930	54040
30	29.7	1800	54000
32	29.7	1720	55040
34	29.7	1650	56100
36	29.7	1540	55440
38	29.7	1490	56620
		Mean	54823
		COV	0.019
24	33.0	2470	59280
26	33.0	2300	59800
28	33.0	2140	59920
30	33.0	2020	60600
32	33.0	1910	61120
34	33.0	1830	62220
36	33.0	1710	61560
38	33.0	1650	62700
		Mean	60900
		COV	0.018
24	36.0	2690	64560
26	36.0	2500	65000
28	36.0	2340	65520
30	36.0	2220	66600
32	36.0	2080	66560
34	36.0	1990	67660
36	36.0	1890	68040
38	36.0	1800	68400
		Mean	66543
		COV	0.020

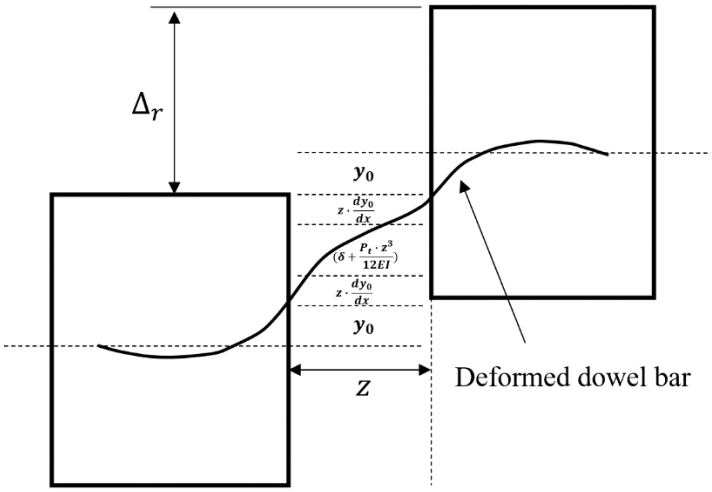

Figure 1. Relative deflection between two concrete blocks.

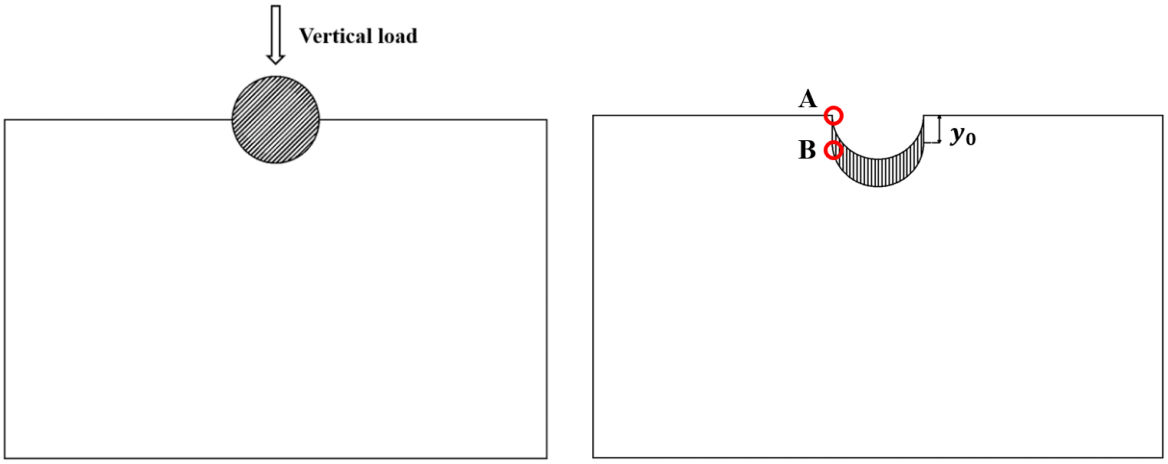

(a) (b)

Figure 2. Vertical deformation of the Winkler concrete foundation (a) dowel bar under vertical load, (b) uniform deformation of concrete dowel slot.

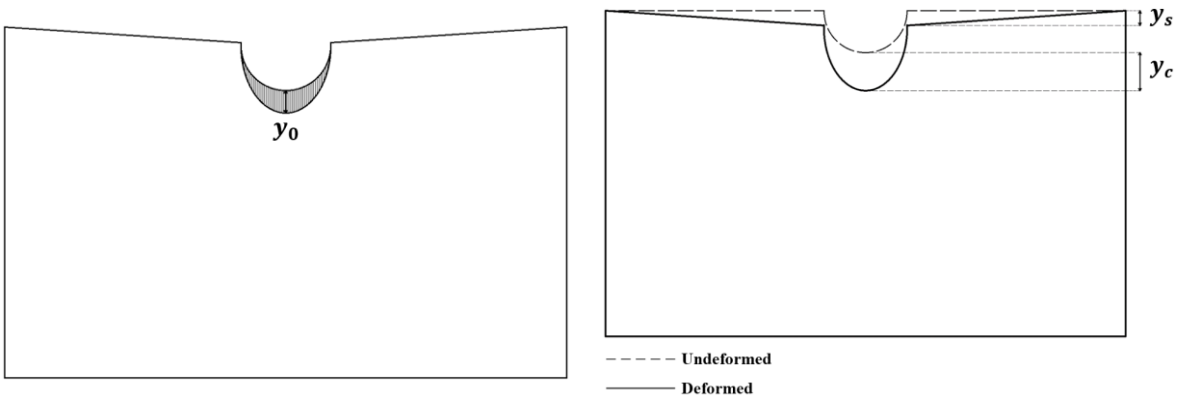

(a) (b)

Figure 3. Deformation of the elastic concrete support under vertical load (a) deformed dowel slot, (b)

deformed and undeformed concrete support.

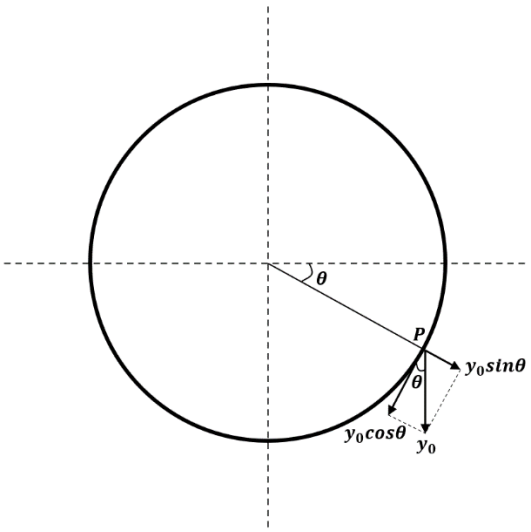

Figure 4. Vertical deflection decomposition.

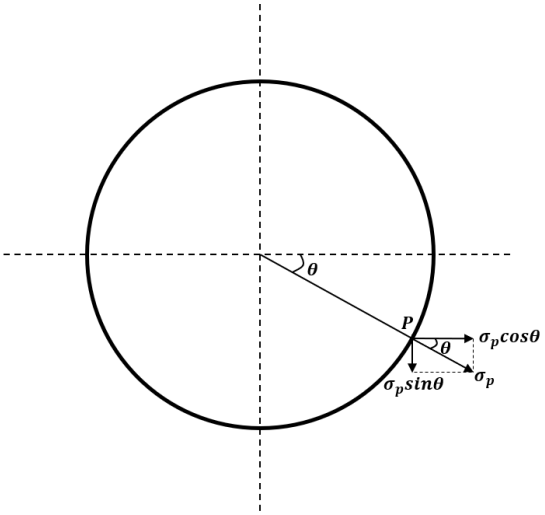

Figure 5. Contact stress decomposition.

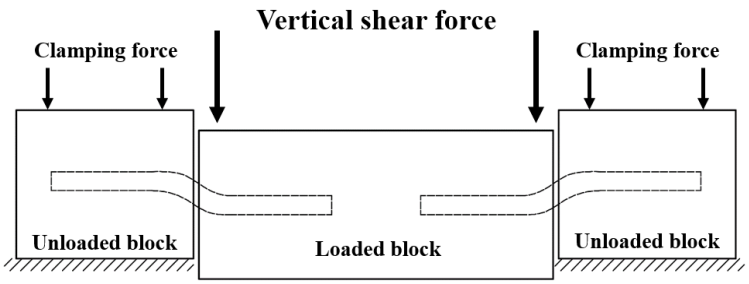

Figure 6. The modified AASHTO T253 method (Porter and Pierson 2007).

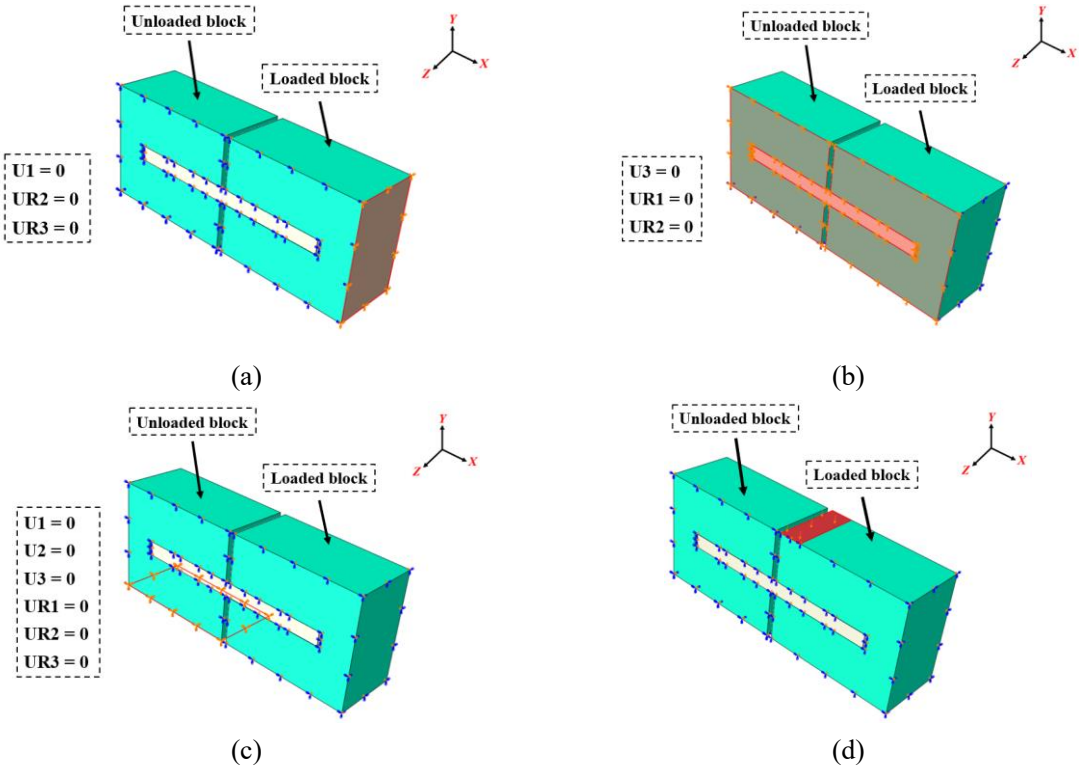

Figure 7. Boundary conditions and the loading arrangement in finite element analysis (a) symmetric constraint along the X direction, (b) symmetric constraint along the Z direction, (c) restriction of the unloaded block, (d) loading arrangement in finite element analysis.

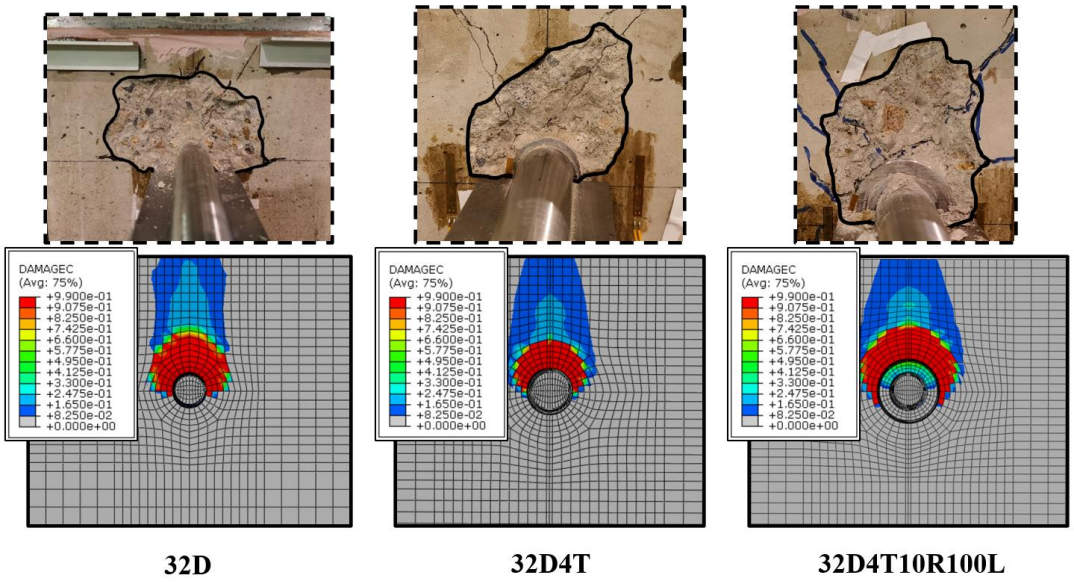

(a)

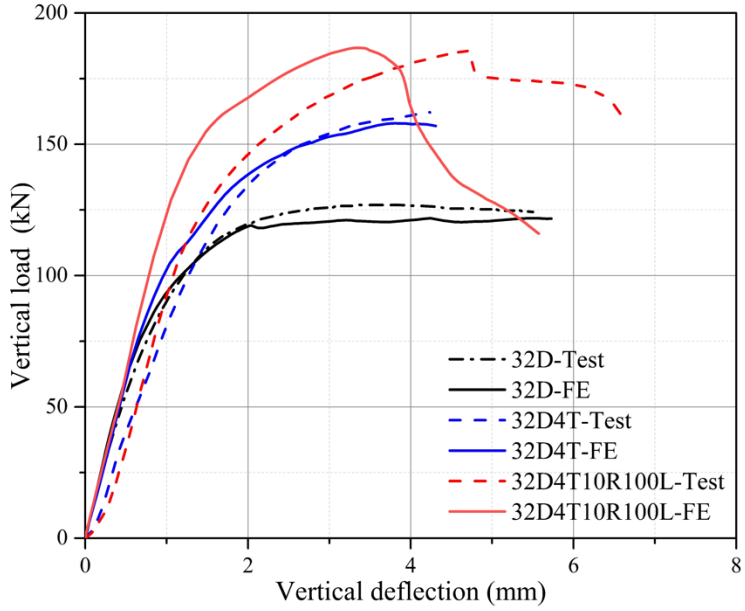

(b)

Figure 8. Validations of the developed finite element model (a) concrete crushing failure, (b) load-deflection curve.

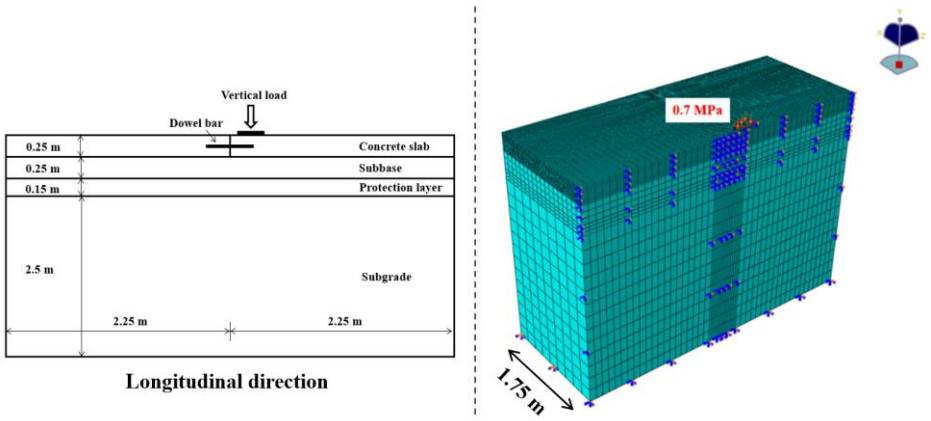

(a)

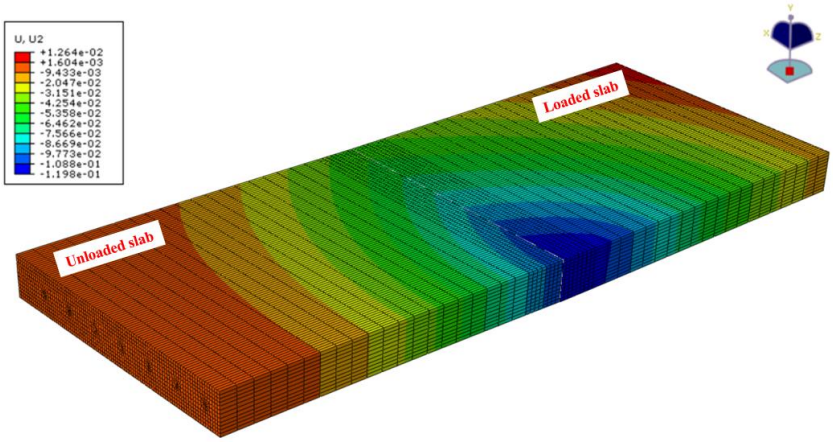

(b)

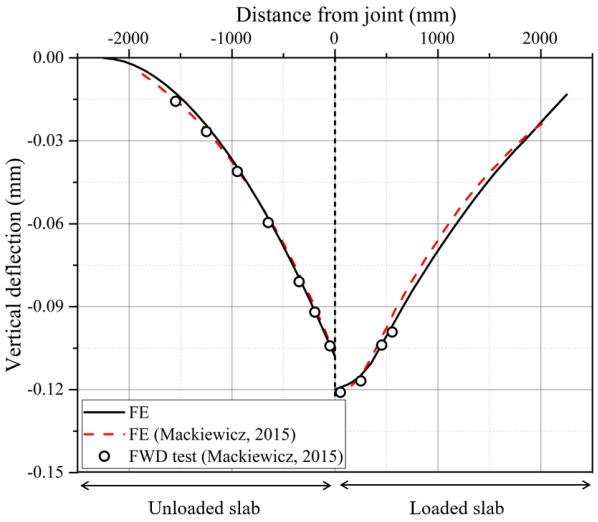

(c)

Figure 9. Full-scale jointed concrete pavement. (a) model dimension and configuration, (b) vertical deflections of concrete slabs (U2), (c) load-deflection curves.

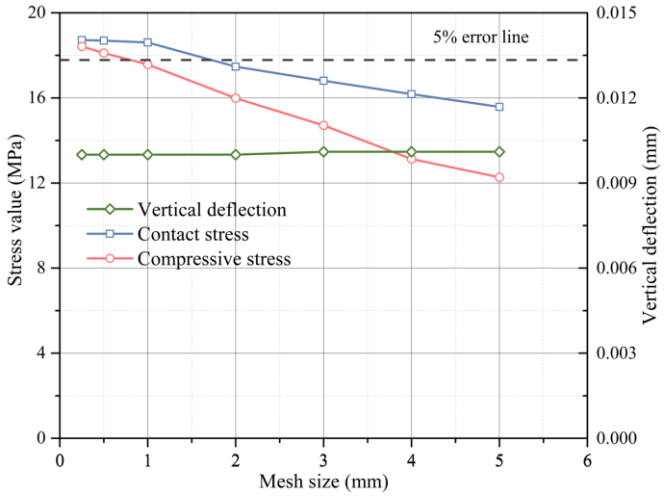

Figure 10. Mesh convergence analysis.

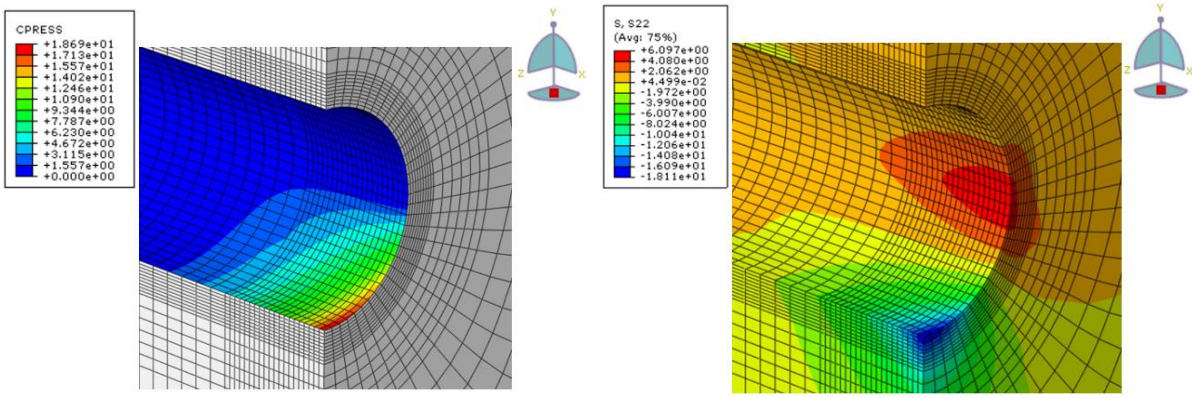

(a) (b)

Figure 11. Normal contact stress (CPRESS) and vertical compressive stress (S22) distributions in the dowel slot of the unloaded block (a) normal contact stress distribution, (b) vertical stress distribution.

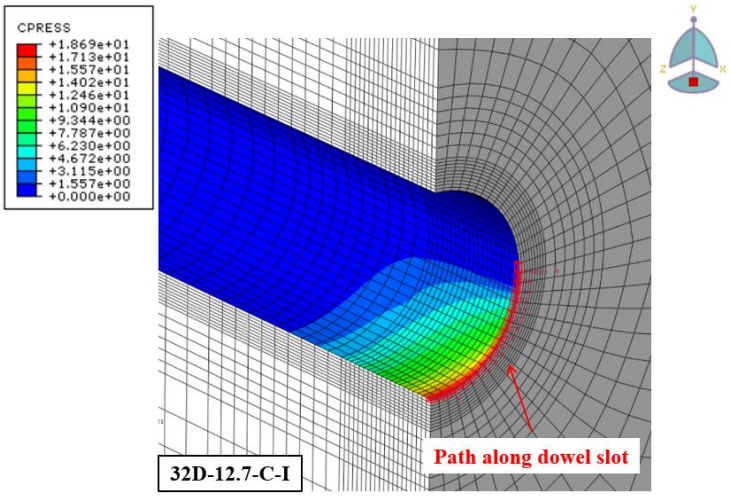

(a)

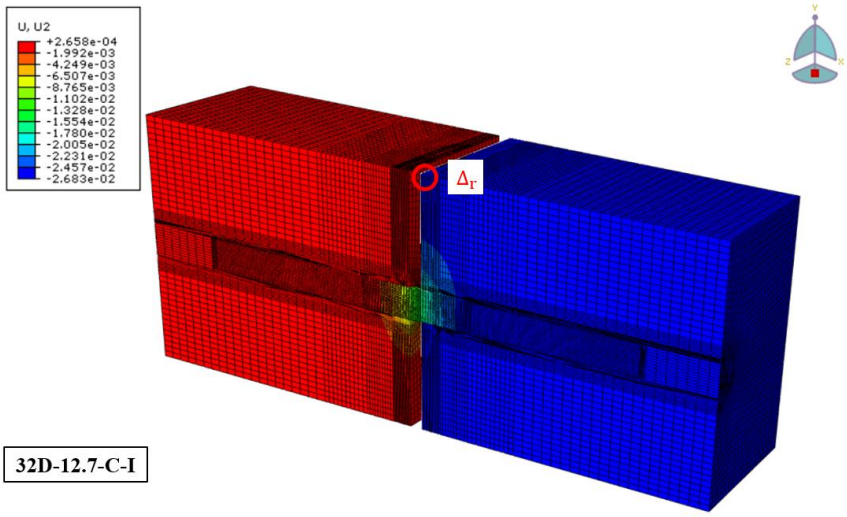

(b)

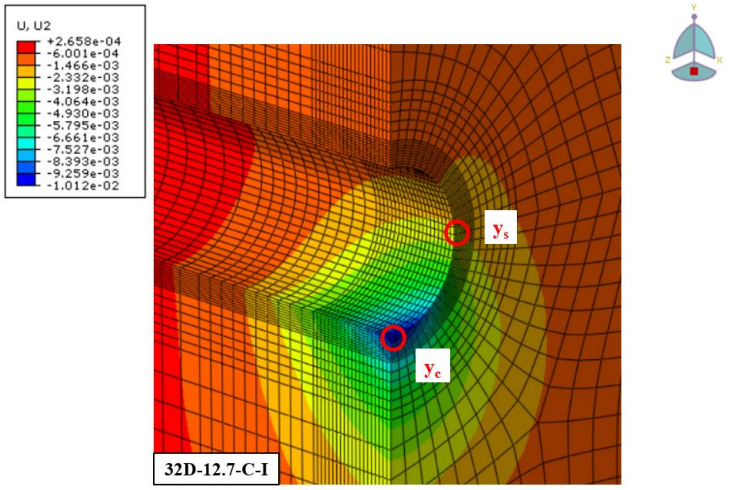

(c)

Figure 12. Stress and deflection data obtained from finite element analysis (a) contact stress distribution, (b) relative deflection between concrete blocks, (c) deflections within dowel slot of unloaded block.

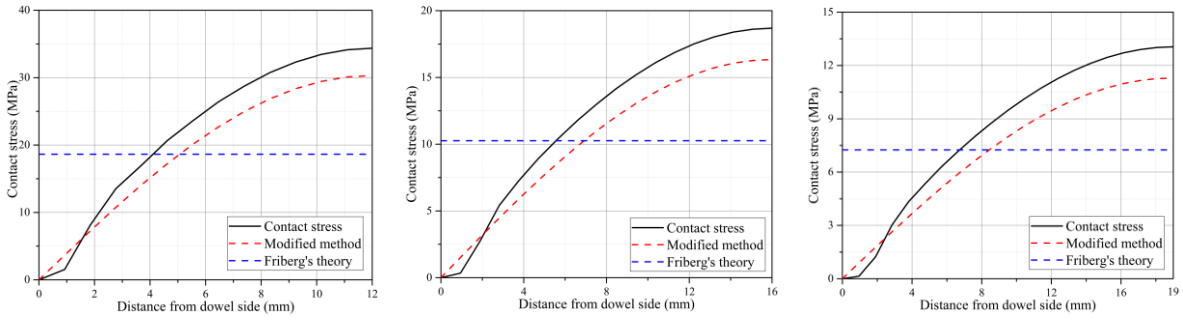

(a) (b) (c)

Figure 13. Contact stress distributions of models with 12.7 mm joint width and C-I concrete (a) 24 mm dowel bar, (b) 32 mm dowel bar, (c) 38 mm dowel bar.

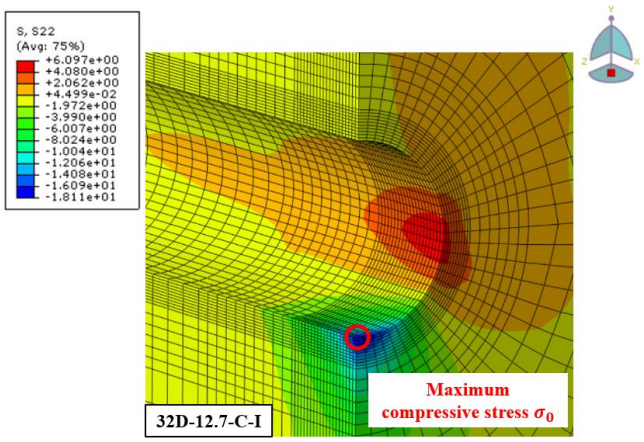

Figure 14. Maximum compressive stress σ_0 in the unloaded block.

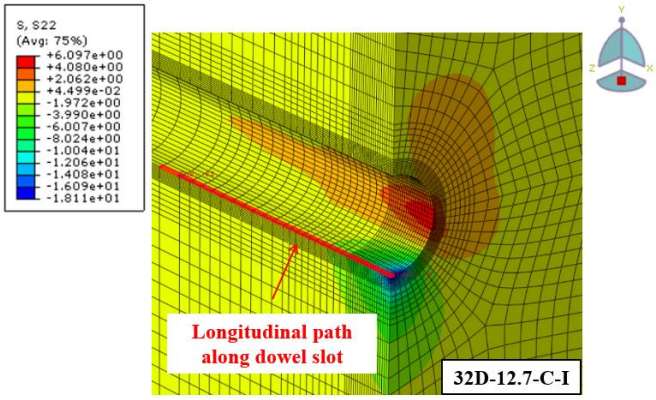

Figure 15. Longitudinal path along the dowel slot.

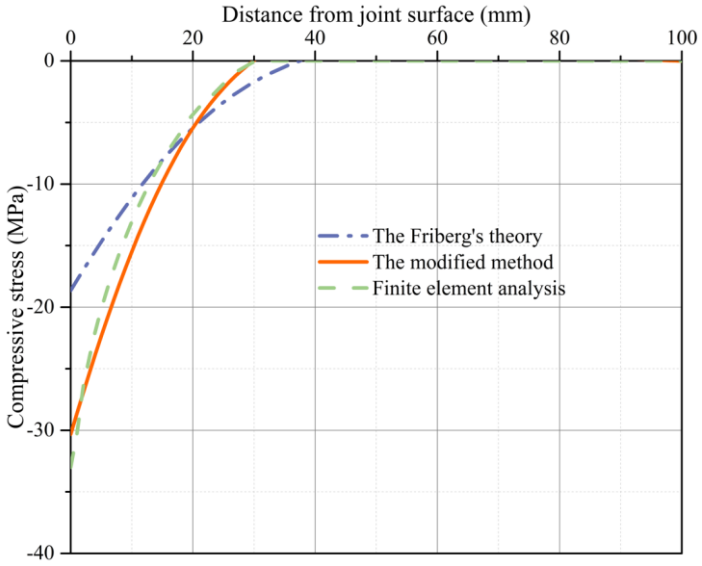

(a)

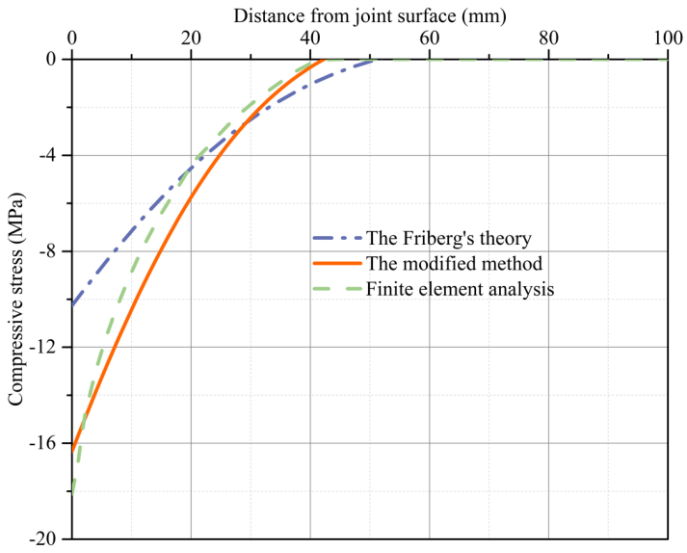

(b)

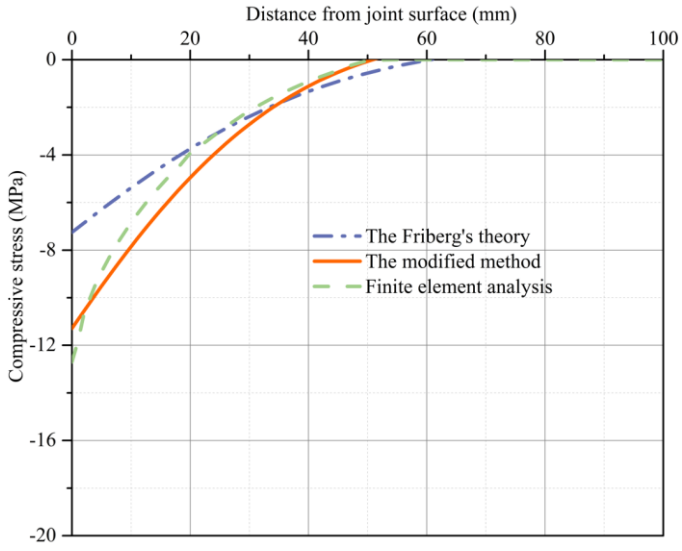

(c)

Figure 16. Longitudinal compressive stress distributions of models with C-I concrete and 12.7 mm joint width (a) 24 mm dowel bar, (b) 32 mm dowel bar, (c) 38 mm dowel bar.

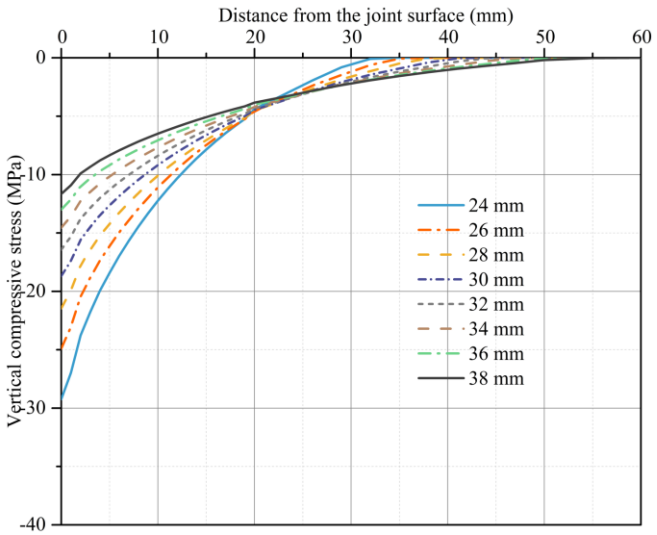

Figure 17. Vertical compressive stress distribution along dowel slot (6.4 mm joint width and C-I concrete).

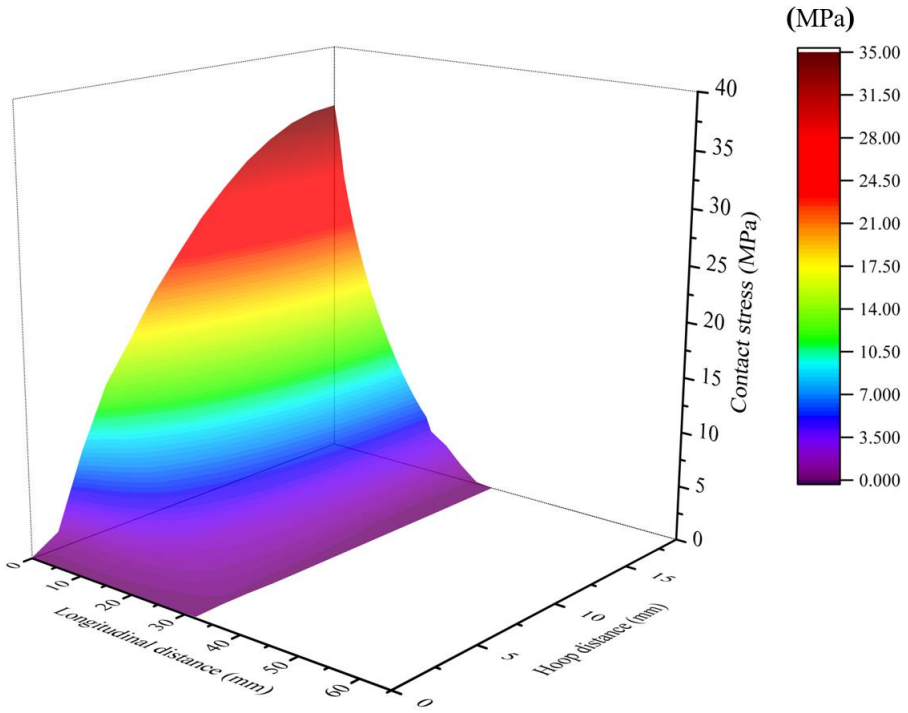

(a)

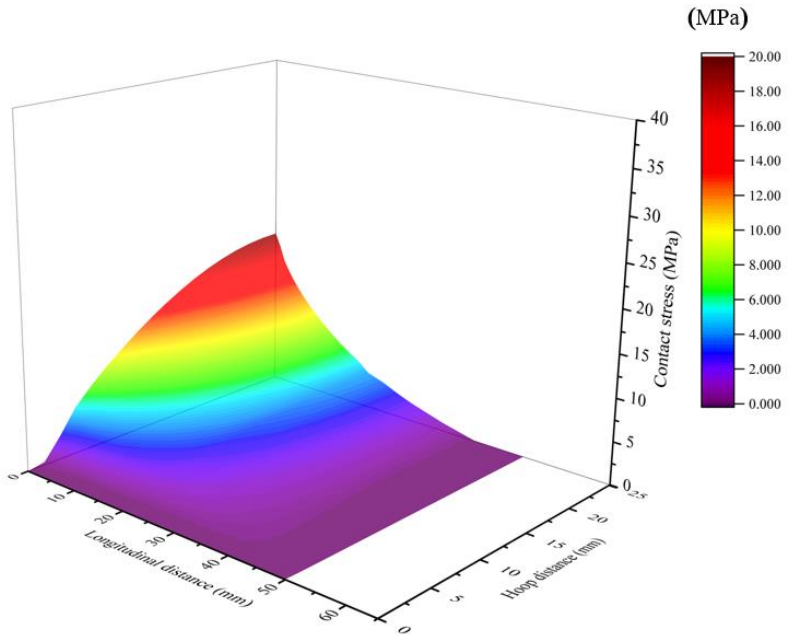

(b)

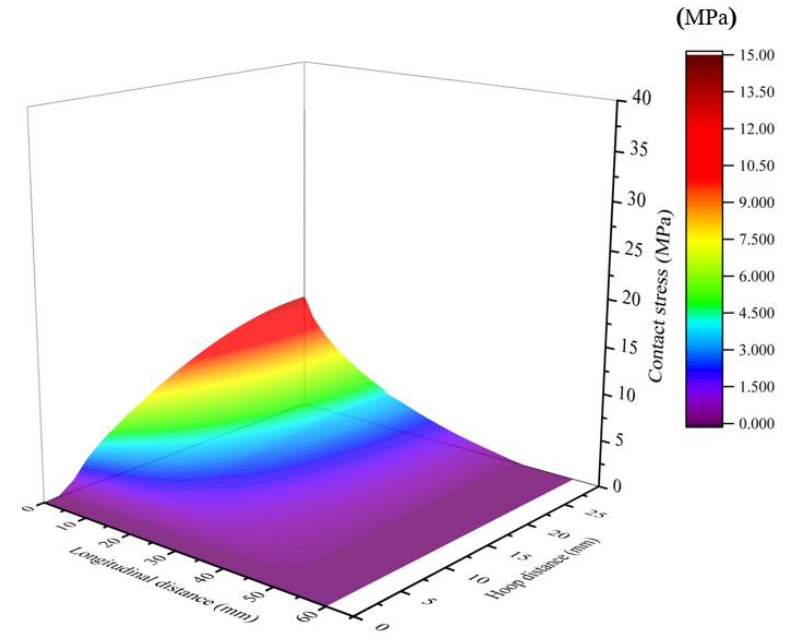

(c)

Figure 18. Three-dimensional contact stress distributions of models with C-I concrete and 12.7 mm joint width (a) 24 mm dowel bar, (b) 32 mm dowel bar, (c) 38 mm dowel bar.

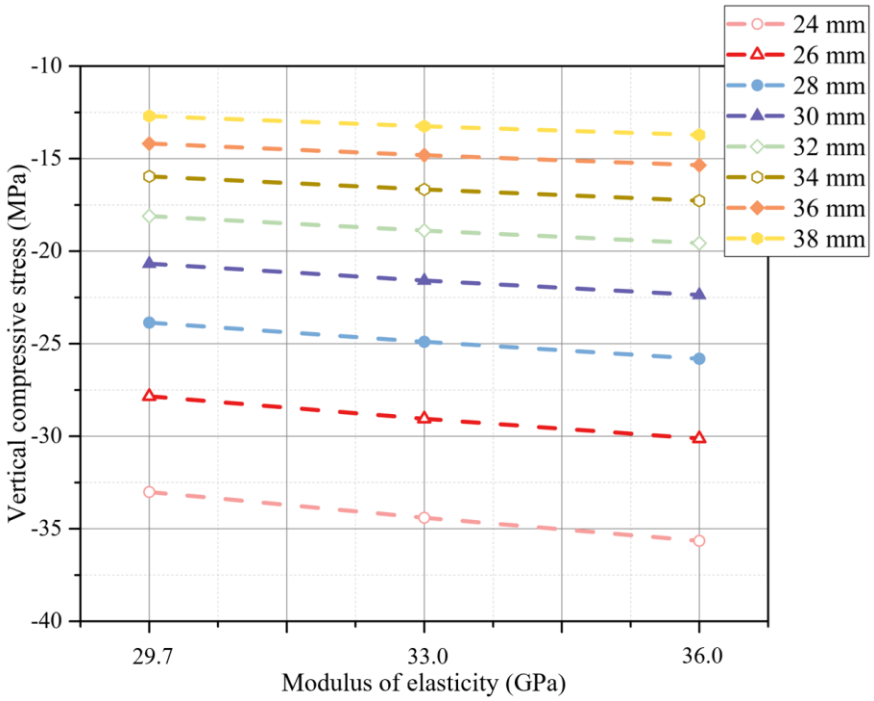

Figure 19. Vertical compressive stress with different types of concrete (12.7 mm joint width).

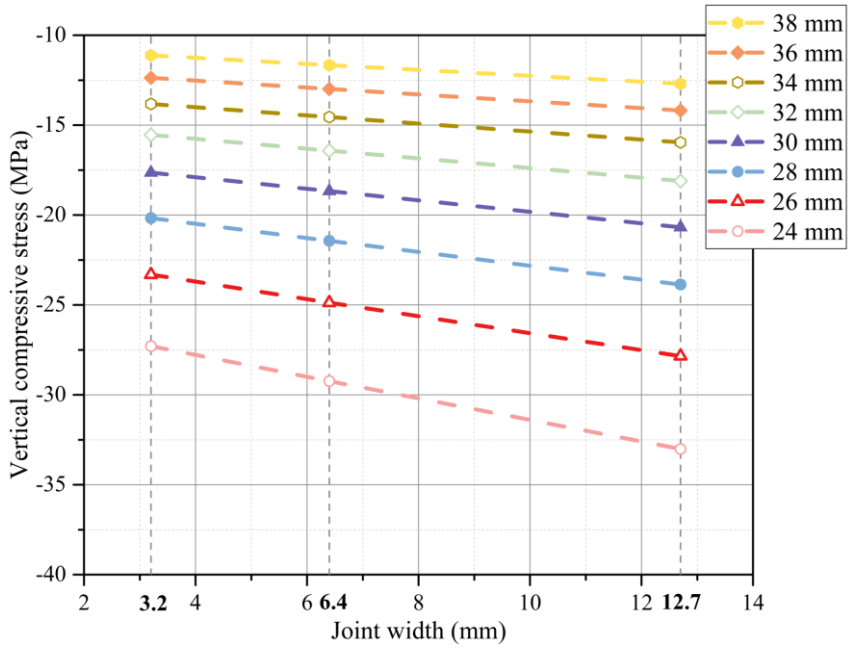

Figure 20. Vertical compressive stress with different joint widths (C-I concrete).

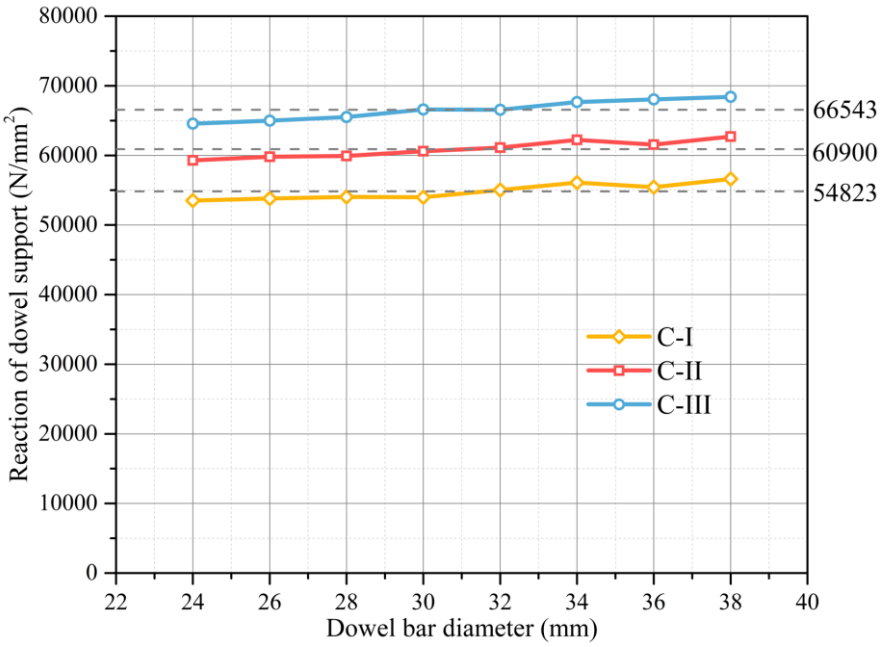

Figure 21. Reaction of concrete dowel slot with different types of concrete.

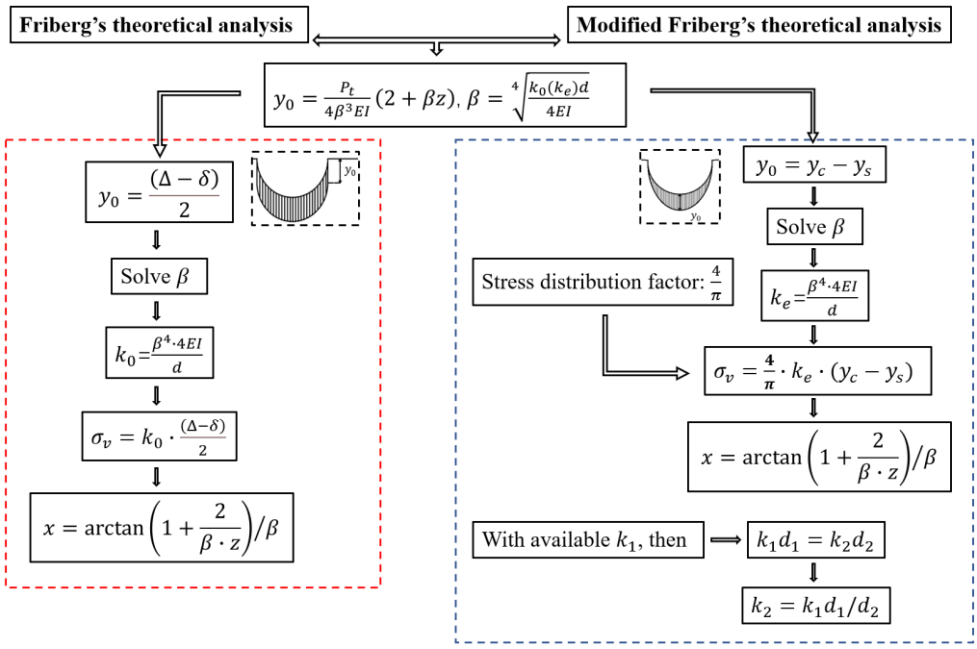

Figure 22. Flow chart of the (modified) Friberg's theoretical analysis.